Ionospheric electrodynamics

Auroral arcs are the simplest auroral forms, typically described in terms of 1D stripes of increased ionospheric conductance (Figure 1a). While the 1D arc model, often realized in the evening and morning sectors of the auroral oval, was studied extensively in the past, real arcs can exhibit 2D features (Figure 1b), for example in the so called Harang region (HR), near the magnetic midnight. The auroral activity in the HR is thought to be closely related to the substorm onset, but the details of this relationship are not fully understood. While meso-scale investigations of HR electrodynamics have been conducted based on ground data, high-resolution satellite data are needed for systematic arc studies. Although at least two satellites are required to check more closely the gradients along the arc (a configuration to be provided soon by the Swarm mission), one satellite data can already provide useful insights, if the assumption of a divergence free electrojet is dropped.

Marghitu et al. (2009a) examined two apparently standard events observed by the FAST satellite and ground facilities in the HR. In both events the current closure at ionospheric level was found to be dominated by the coupling between the FAC and the electrojets (EJ) over significant fractions of the auroral oval, with potentially important implications for the auroral current circuit and M–I coupling. Figure 2 presents one of these events, with input/output data on the left/right side. Based on the input data, the ALADYN technique (*Marghitu et al., J. Geophys. Res., 2004*), provided detailed information on the ionospheric electrodynamics, including the tangential electric field, b_0, and the electrojet divergence, c_1. In our case c_1 quantifies with good approximation the FAC–EJ coupling. The application of ALADYN shows that the large-scale upward and downward FACs are essentially decoupled in the ionosphere near the footprint of the satellite path. Poleward of the convection reversal (CR) boundary (indicated in the two bottom panels of Figure 2) the westward EJ feeds the upward FAC associated with a wide and stable auroral arc, while equatorward of the CR the eastward EJ appears to be fed by the downward FAC. The coefficient c_1 was found to be equal with 0.4 $\mu A/m^2$ over the interval I1 and with -1.5 $\mu A/m^2$ over the interval I2 (see Figure 2 for I1 and I2), roughly equal with the respective average FAC densities. This was interpreted as a strong indication for the FAC–EJ coupling.

In order to speed up the data analysis, Costel Bunescu equipped the ALADYN routines with a graphical interface, assembling thus the XALADYN software package. By using this package, it became clear that the search for b_0 and c_1 was not systematic enough in the fit procedure implemented by ALADYN. A systematic scan of these two key quantities in the parameter space was implemented by an update version of the ALADYN technique *Marghitu et al., 2011a*. In this case, the fit equation is solved over a sliding window, assuming a divergence free electrojet, $c_1 = 0$, for a set of b_0 values covering the range of tangential electric field values typical for auroral arcs. By quantifying the quality of the fit and the deviation of the results from the assumption of a divergence free electrojet, one can obtain both an estimate for the tangential electric field and a profile of the actual c_1. Results obtained with the updated ALADYN technique for the event presented in Figure 2 are illustrated in Figure 3. Further examination of this event, complemented by an analytic approach, enabled a more complete view on the FAC ionospheric closure, as provided by Pedersen and Hall currents across and along the arc. A tentative scenario for the arc evolution during the substorm cycle emerged from this analysis, suggesting relationships between various arc features and the substorm stages. The systematic review of various arc models performed by *Marghitu, 2012* provided a more structured framework to address this scenario.

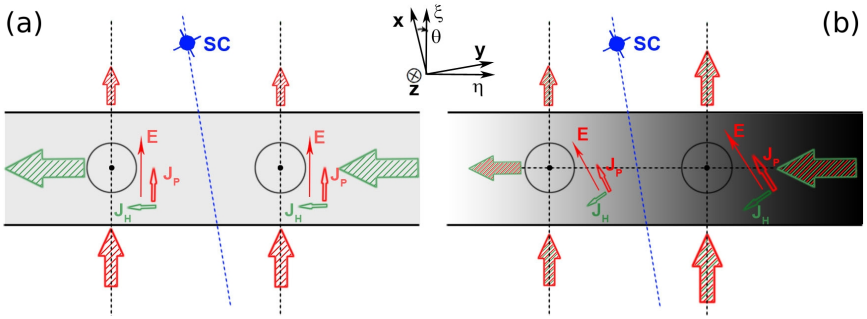

Figure 1: The 1D (a) and 2D (b) arc models (from *Marghitu et al., 2011a*). The conductance, FAC, ionospheric electric field, and ionospheric current are indicated by the gray shade, circles, solid arrows, and hatched arrows respectively. Red and green show the Pedersen and Hall components of the current. For the 1D arc, that can be explored by one satellite, the electric field drives a Pedersen current normal to the arc, closed by FAC, and a divergence free Hall electrojet. For the 2D arc, the electrojet is no longer divergence free, because of the gradients in conductance and electric field along the arc. While a close examination of these gradients requires at least two satellites, useful insights can be obtained also from one satellite data, if the assumption of a divergence free electrojet is dropped.

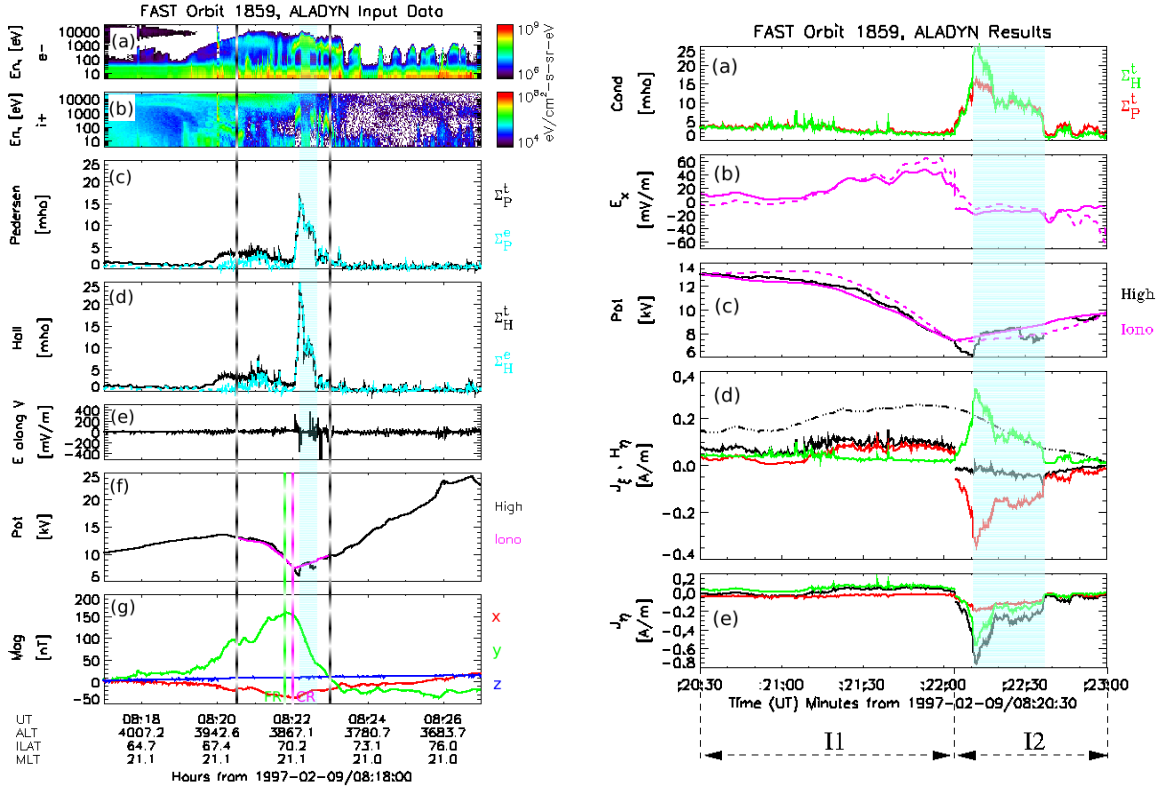

Figure 2: *Left:* Selection of FAST particle and field data: Electron (**a**) and ion (**b**) energy spectrograms; Pedersen (**c**) and Hall (**d**) conductance; high altitude electric field parallel to the satellite velocity (**e**); high altitude potential drop along the satellite track (**f**); perturbation magnetic field (**g**). In the panels (**c**) and (**d**) the total/electron conductance is shown black/cyan. The dashed vertical lines indicate the ALADYN application interval, 8:20:30–8:23:00 UT. The visible arc is shown with the cyan band. The dashed magenta and green lines in the two bottom panels indicate the convection and field-aligned current reversal, respectively (CR and FR). *Right:* Electrodynamic parameters from 8:20:30–8:23:00. ALADYN was applied separately over the sub-intervals I1 and I2, equatorward and poleward of the CR. The quantities from top to bottom are: (**a**) Pedersen and Hall conductance; (**b**) ionospheric electric field E_x obtained for a westward electric field, $b_0 = 12$ mV/m, and a divergent ($c_1 \neq 0$, solid), respectively divergent free ($c_1 = 0$, dashed) electrojet; (**c**) ionospheric potential (magenta, same line styles as in b) and high altitude potential (black); (**d**) Ionospheric current J_ξ (black, solid), together with its Pedersen (red) and Hall (green) components, as well as the field-aligned sheet current, H_η (black, dash-dotted); (**e**) J_η current, same colors as J_ξ. The currents J_ξ and J_η are shown only for the case $c_1 \neq 0$, when the match between the ionospheric and high altitude potential is better.

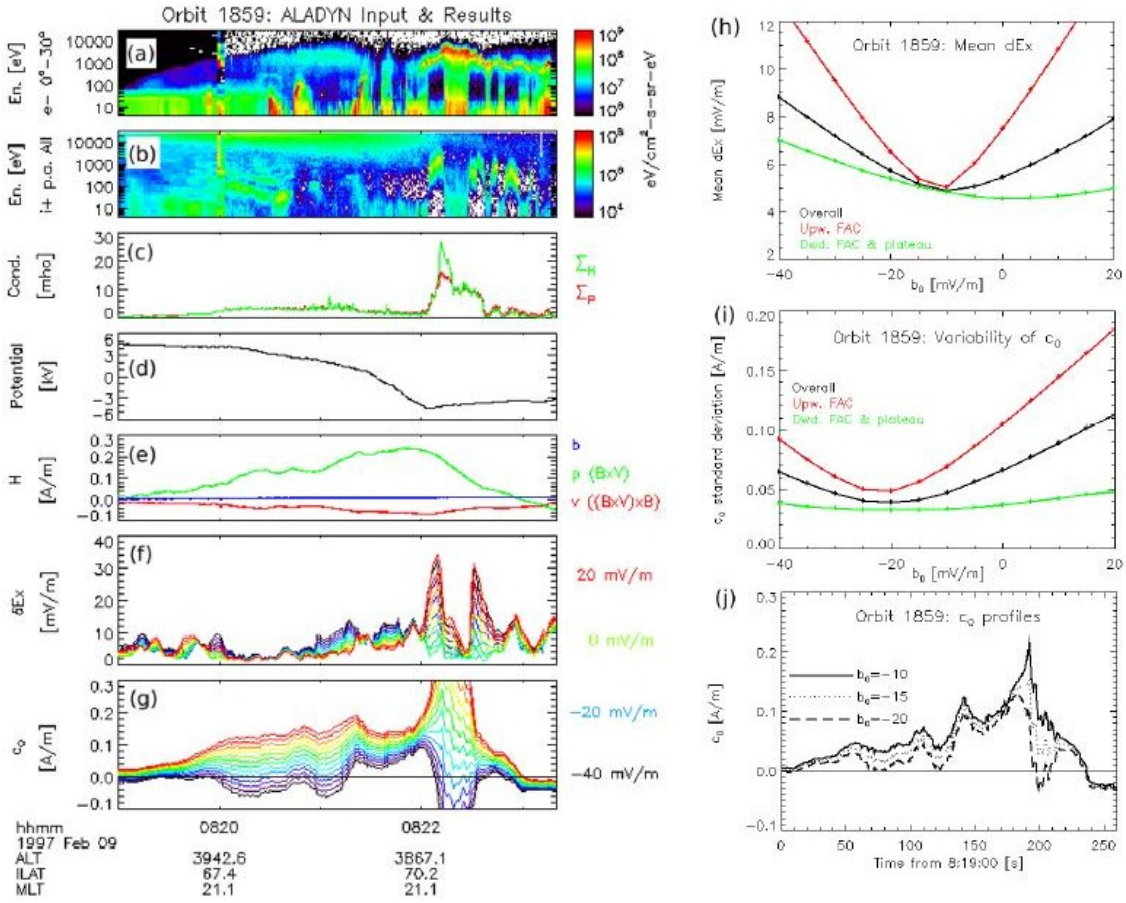

Figure 3: Examination of the FAST event from Figure 2 by the updated ALADYN technique. After Figures 3 and 4 of *Marghitu et al., 2011a*. *(a)–(e):* FAST data. (a) Electron and (b) ion time–energy spectrograms; (c) Pedersen and Hall conductance; (d) ionospheric potential along the FAST footpoint; (e) magnetic field perturbation. *(f)–(j):* ALADYN results. (f) Difference between the fitted electric field and the mapped electric field measured by FAST, δE_x, for b_0 between -40 mV/m (westward) and 20 mV/m (eastward), varies in steps of 5 mV/m; (g) Background meridional ionospheric current, c_0, for the same set of b_0 values; c_0 should be constant if the electrojet divergence is indeed 0; (h, i) Mean δE_x and standard deviation of c_0, computed for each line in (f) and (g), respectively, over the whole FAC region (black), upward FAC (red), and downward FAC (green); (j) The c_0 profile for $b_0 = -20$, -15, and -10 mV/m.